IEEE Access
Multidisciplinary | Rapid Review | Open Access Journal

Received July 10, 2020, accepted July 27, 2020, date of publication August 4, 2020, date of current version August 17, 2020.

Digital Object Identifier 10.1109/ACCESS.2020.3014120

Design and Analysis of the Multifunctional Oil-Injection Equipment for Deep-Sea Hydraulic Systems

HAOCAI HUANG[1,2,3], CHENGCHENG ZHU[1], WENJUN ZHANG[4], SHUAI HAO[1], SHUQING ZHANG[1], JIANXING LENG[1], AND YAN WEI[1,3], (Member, IEEE)

[1]Ocean College, Zhejiang University, Zhoushan 316021, China
[2]Laboratory for Marine Geology, Qingdao National Laboratory for Marine Science and Technology, Qingdao 266061, China
[3]Key Laboratory of Ocean Observation-Imaging Testbed of Zhejiang Province, Zhejiang University, Zhoushan 316021, China
[4]College of Shipbuilding Engineering, Harbin Engineering University, Harbin 150001, China

Corresponding author: Yan Wei (redwine447@zju.edu.cn)

This work was supported in part by the National Natural Science Foundation of China under Grant 41576031 and Grant 61901410, and in part by the Science and Technology Projects of Zhoushan Municipal Science and Technology Bureau for Zhejiang University under Grant 2019C81035.

ABSTRACT Hydraulic systems have been frequently used in deep-sea equipment because of their renowned long service life, stable and reliable performance. However, impurities contained in hydraulic oil, such as solid particles, gas and water, would jeopardize work efficiency of deep-sea hydraulic systems, and in some extreme cases even cause failure of the whole system, resulting in breakdown of crucial deep-sea equipment. Therefore, this paper aims to present a device, multifunctional oil-injection equipment (MOIE), expected to be able to purify hydraulic oil in deep-sea hydraulic systems. Its major functions are to absorb oil, remove impurities and fill oil, among which the removal of water and gas, i.e. dewatering and degassing, is of significance. Theoretical analysis shows that the paper oil filter is able to remove the solid particles in hydraulic oil, and degassing and dewatering of hydraulic oil could be achieved through vacuum filtration and vacuum heating in high-temperature and low-pressure environment. The prototype of the MOIE is designed and manufactured. The results from laboratory experiments indicate that this equipment can effectively remove solid particles, gas and water from hydraulic oil. This study ensures the stability, safety and reliability of the deep-sea hydraulic system by improving the quality of hydraulic oil.

INDEX TERMS Deep-sea hydraulic systems, degas, dewater, oil-injection, pressure tank, vacuum heating, vacuum filtration.

I. INTRODUCTION

In deep-sea hydraulic systems, pressure compensation devices are commonly used to mitigate the influence of sea water pressure on systems [1]. Hydraulic oil is an ideal pressure-balancing medium in deep-sea pressure compensation devices [2]. The main impurities in hydraulic oil are solid particles, gas, and water [3]. The impurities would affect the performance of hydraulic systems, shorten service life of hydraulic components, and sometimes even be the critical factor to determine whether hydraulic systems can work normally [4], [5]. Solid particles in hydraulic oil could easily wear and block hydraulic devices [6]. Gas in it would significantly increase compressibility and non-linearity of hydraulic oil, which will affect the accuracy and rigidity of system transmission, leading to undesirable consequences such as actuator movement errors, automatic control errors, inaccurate positioning, and positioning drift [7], [8]. Moreover, water would corrode hydraulic devices and influence insulation performance [9], [10]. Therefore, the purity of hydraulic oil, which means low gas content, low water content and few solid particles must be strictly controlled and guaranteed.

The removal of bubble in hydraulic oil has been considered in design and manufacturing processes of hydraulic systems. To degas, the most commonly used method is to change parameters or shapes of an oil tank in hydraulic systems. For example [11], [12], make sure the horizontal cross-sectional

The associate editor coordinating the review of this manuscript and approving it for publication was Hiram Ponce.

area of oil tank is larger than its vertical cross-sectional area; enlarge the distance between an oil inlet and outlet to make oil flow smoothly; set up a bulkhead in an oil tank and increase its volume to prolong fuel residence time in the fuel tank; reduce the diameter of an inlet and outlet ports to control oil flow [12], [13]. These methods allow oil to move smoothly and stand for a period of time, which contributes to both reducing bubble generation and increasing bubble release time. However, the degassing effect of these methods still needs to be improved because bubble is too small to float to oil surface with its own buoyancy [14]. Although the proposed centrifugal degassing method is relatively simple, it remains challenging to achieve in engineering application [15]. As to water in hydraulic oil, it can be divided into three types: free water, emulsified water and dissolved water, among which dissolved water is difficult to remove [16], [17]. The traditional water removal methods, such as gravity center method, centrifugation method, adsorption method, etc., are not able to remove dissolved water successfully [18]. So, to tackle dissolved water, new methods are needed. At present, specific research on removing gas, water and solid particles in hydraulic oil has hardly been found or is still under way. And few equipment that integrates oil absorption, impurities removing and oil injection has been found or is under development, either. In this paper, we design and develop a multifunctional oil-injection equipment (MOIE) for deep-sea hydraulic systems. It integrates the functions of oil absorption, impurities removing and oil injection, among which impurity removal includes removing solid particles, degassing and dewatering. Its degassing and dewatering of hydraulic oil are achieved through vacuum filtration and vacuum heating in high temperature and low-pressure environment. The following are its advantages:

1) The removal of impurities in hydraulic oil ensures the stability and reliability of the deep-sea hydraulic system.

2) Compared with traditional methods, the oil filtration, impurity removal and oil injection in the MOIE are performed in a closed environment, which avoids secondary pollution.

3) The method of the vacuum oil injection can prevent the air remaining in the deep-sea hydraulic system from contaminating the hydraulic oil.

After a brief introduction, the remainder of this paper is structured as follows. In Section II, the method of removing solid particles, degassing and dewatering are elaborated. In Section III, the design of the MOIE, especially its pressure tank is explained in detail. In Section IV, the degassing and dewatering laboratory experiments are conducted to verify the MOIE oil-filtering performance. The concluding remarks are given in Section V.

II. METHOD OF REMOVING IMPURITIES

The section II mainly introduces the application of high-precision oil filter to remove solid particles from hydraulic oil, and the removal of gas and water by vacuum heating the hydraulic oil in high temperature and low-pressure environment.

A. REMOVING SOLID PARTICLES

The role of an oil filter is mainly to remove solid particles from hydraulic oil. The filtration accuracy of oil filter refers to the size of smallest solid particles that can be filtered out. The oil filter can be divided into rough oil filter ($10 \leq d < 100\mu$m), ordinary oil filter ($5 \leq d < 10\mu$m), high-precision oil filter ($1 \leq d < 5\mu$m), and ultra-precision oil filter ($d < 1\mu$m), where d is the diameter of the smallest solid particles [19]. The commonly used oil filters are listed in Table 1 [20].

Theoretically, the more accurate an oil filter is, the cleaner hydraulic oil and the more reliable hydraulic systems are. But pursuing excessive filtering accuracy alone is unrealistic. For example, hydraulic oil with solid particles less than 1μm is mainly used in ultra-precision instruments, while most ocean equipment does not need such precision hydraulic oil and $3 \sim 5\mu$m can well meet the requirements. Moreover, such ultra-precision oil filter is not available on market and needs to be tailor-made. The selection of oil filter should consider other factors as well, such as filtration accuracy, cleaning method, flow capacity, service life, etc. [21]. The oil filtering accuracy is expected to be $2 \sim 10\mu$m. Therefore, compared with metal oil filter, paper oil filter is selected for the following two reasons: first, since oil flow rate is not high, it does not require filter to have high strength; second, paper oil filter can absorb some water in the oil while filtering the solid particles at the same time. Furthermore, metal filter is difficult to clean and replace when it is clogged. Fig. 1 is the structure scheme of a paper oil filter. The oil enters in inlet A, passes through filter core and flows out of outlet B. In this process, solid particles are filtered and cling to the surface of filter paper. When the pressure difference between m and n, signifying the pressure at the inlet and the outlet respectively, reaches a preset value, the signal generator sets an alarm to remind people to replace the filter core. And the filter core should be changed frequently in case being blocked and affecting the filtering accuracy.

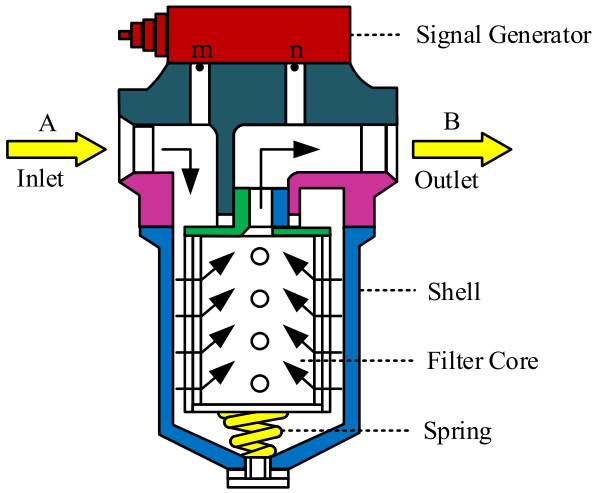

FIGURE 1. Structure scheme of paper oil filter.

TABLE 1. Commonly used oil filters.

Oil filter	Type	Filtration accuracy(d/μm)	Filter core	Characteristics
Mesh oil filter	Rough	$20 \leq d < 100$	Copper-mesh	Simple structure, Easy to clean, high strength
Line-gap oil filter	Ordinary	$5 \leq d < 10$	Steel wire or aluminum wire	Simple structure, Not easy to clean
Paper oil filter	High-precision	$3 \leq d < 5$	phenolic resin or microporous wood pulp	Lower cost, Easy to clean, Not high strength, able to absorb a small amount of water in oil
Metal oil filter	High-precision	$3 \leq d < 5$	Sintered metal powder	Difficult to clean, high strength

TABLE 2. Description of parameters.

Notation	Description	Notation	Description
R	Radius of the gas-nucleus	N	Content of the gas-nucleus
R_0	Original radius of the gas-nucleus	γ	Heat capacity ratio
R_c	Critical radius of the gas-nucleus	σ	Cavitation inception coefficient
P_g	Pressure on the gas-nucleus	P_v	Standard atmospheric pressure
P_c	Critical pressure on the gas-nucleus	P_b	Pressure of the bubble
r	Radius of the bubble	F_r	Viscous resistance of the bubble
h	Depth of the bubble	a	Rising acceleration of the bubble
ρ_g	Density of the bubble	P_0	Oil-surface pressure
ρ_l	Density of the oil	V_b	Volume of the bubble
m	Mass of the bubble	n_b	Amount of substance of the bubble
F_g	Gravity of the bubble	R_m	Gas constant
F_b	Buoyancy of the bubble	T	Temperature
v	Rising speed of the bubble	M_b	Molar mass of the bubble
u	Oil fluid viscosity	t_d	Rising time of the bubble

B. DEGASSING

Degassing means removing gas-nucleus and bubble from hydraulic oil. Gas-nucleus is microscopic while bubble is macroscopic [22], [23]. Increasing the radius of gas-nucleus can cause it to develop into bubble [24]. Here, we first explain in what kind of environment would gas-nucleus develop into bubble. Then, theoretic analysis is presented to describe rising motion of bubble in hydraulic oil, and we particularly look into how oil fluid viscosity influences bubble rising movement.

The gas-nucleus scale distribution spectrum is applied to indicate the content of gas-nucleus with different radius in the liquid [25]. It is challenging to theoretically study the gas-nucleus scale distribution spectrum since too many factors are intertwined, and currently it is difficult to derive. Through fitting a large number of experimental data, Pan obtained an empirical formula of the gas-nucleus scale distribution spectrum in the liquid at standard atmospheric pressure [26]–[28]:

$$N = 864e^{-\frac{12}{R}}R^{-4} \tag{1}$$

The description of all parameters mentioned from Eq.s (1) - (20) in Chapter B is provided in Table 2, where R is the radius of gas-nucleus and N is the content of gas-nucleus. This formula is highly consistent with the experimental data of the Ginedroz's gas-nucleus scale distribution, and is considered reliable [29], [30]. The gas-nucleus scale distribution spectrum shown in Fig. 2 is plotted from Eq. (1). It shows that the radius of gas-nucleus is mainly distributed in $1 \sim 30\mu$m. When $R \geq 30\mu$m, the gas nucleus content is almost zero. Set G as the content of gas-nucleus in the liquid when $R \geq x$ (x is a positive number on the X axis). To calculate G, Eq. (1)

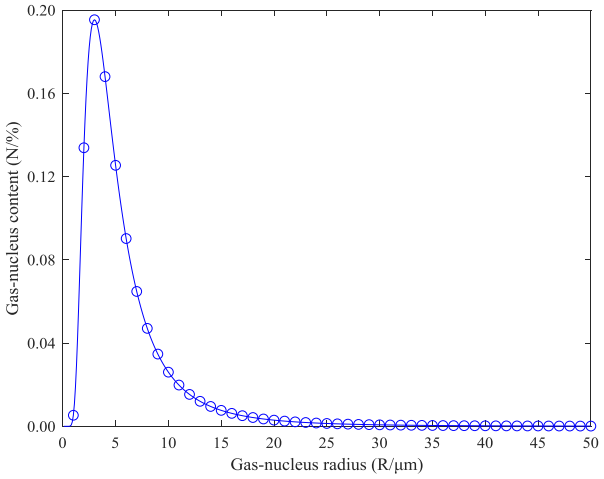

FIGURE 2. Gas-nucleus scale distribution spectrum.

needs to be rewritten as follows:

$$G = 1 - \int NdR \tag{2}$$

Let $R = 1\mu$m be substituted into Eq. (2) to obtain $G = 99.95\%$, which means that the radius of almost all gas-nucleus in the liquid is greater than 1μm.

For easy analysis, let gas-nucleus and bubble be ideal gas. According to idea gas equation:

$$PV = nR_{\mathrm{m}}T \tag{3}$$

where P is the absolute pressure, V is the volume of ideal gas, n is the amount of substance of ideal gas, T is the absolute temperature, and R_m is the molar gas constant. Since n does not change, increasing T and decreasing P together would cause V to increase. This can be explained by the fact that in high-temperature and low-pressure environment, molecules move violently and the distances among them become larger, i.e. the radius of gas-nucleus R continues to increase [31]. As the process of gas-nucleus developing into the bubble illustrated in Fig. 3 shows, when $R \geq R_c$, the gas-nucleus would lose its stability and develop into bubble. Then R_c is the maximum radius at which the gas-nucleus remains stable. Gas-nucleus with different R_o have different R_c [32]. Therefore, the prerequisite for gas-nucleus to develop into bubble is $P_g < P_c$ [33].

Eq. (4) is the critical pressure equation of gas-nucleus [34], [35]:

$$P_c = \frac{2\sigma(1-3\gamma)}{3R_o\gamma} + P_v \tag{4}$$

where γ, P_v, and σ are the constants, $\gamma = 1.4$, $P_v = 101.325$kPa and $\sigma = 0.05$. The radius of almost all gas-nucleus in the liquid is greater than 1μm, so bring $R_c = 1\mu$m into Eq. (4) to obtain $P_c = 2.513 \times 10^4$ Pa. Vacuum means low-pressure. In this paper, vacuum refers to the middle level of vacuum degree, between 1.333×10^{-1}Pa and 1.333×10^3Pa. Since 1.333×10^3Pa $< 2.513 \times 10^4$Pa, it is concluded that in high-temperature and vacuum (HTV) environment, gas-nucleus will develop into bubble.

After gas-nucleus develops into bubble, its ascending velocity in oil is similar to the descending velocity of solid particles in liquid [36], [37]. The external force of bubble and solid particle are the same but in opposite directions, which easily causes bubble to deform [38]–[40]. Therefore, the bubble is approximated to an equal volume of solid sphere for analysis [41]–[43].

The Stokes' law is:

$$F_g = \frac{4}{3}\pi r^3 \rho_g \mathrm{g} \tag{5}$$

$$F_b = \frac{4}{3}\pi r^3 \rho_l \mathrm{g} \tag{6}$$

$$F_r = 6\pi\mu r v \tag{7}$$

According to Newton's law:

$$F_b - F_g - F_r = ma \tag{8}$$

substitute Eqs. (5) - (7) into Eq. (8):

$$\frac{4}{3}\pi r^3(\rho_l - \rho_g)g - 6\pi u r v = \frac{4}{3}\pi r^3 \rho_g a \tag{9}$$

When $v = 0$, the bubble is in its initial state and its rising acceleration reaches the maximum, i.e. $a = a_{max}$. When $a = 0$, the bubble is in an equilibrium state and its rising speed takes the maximum value, i.e. $v = v_{\max}$. After $a = 0$, the bubble rises with a constant speed v_{max}, as illustrated in Fig.4. Therefore, the acceleration motion causes v from the starting 0 to reach v_{max}, and the uniform motion is $v = v_{max}$. The time for the acceleration motion is t_d and that for the uniform motion is t_s.

Integrate the separation variable for Eq. (9):

$$v = (v_0 - \frac{2(\rho_l - \rho_g)gr^2}{9u})e^{-\frac{9u}{2\rho g r^2}t} + \frac{2(\rho_l - \rho_g)gr^2}{9u} \tag{10}$$

Substituting $a = 0$ into Eq. (9) is

$$v_{\max} = \frac{2}{9u}gr^2(\rho_l - \rho_g) \tag{11}$$

From Eqs. (10)- (11), when $v = v_{max}$:

$$y = \frac{2(\rho_l - \rho_g)gr^2}{9u}e^{-\frac{9u}{2\rho g r^2}t_d} = 0 \tag{12}$$

Therefore, the smaller the bubble radius r is, the shorter the acceleration time t_d is. At standard atmospheric pressure ($T = 273.16$K, 101.325kPa), $\rho_g = 1.293$kg/m^3, fluid viscosity of NO.46 anti-wear hydraulic oil is $u46 = 0.0391$Pa.s, the radius of most bubble in hydraulic oil is below 1.5×10^{-4}m and a few larger bubble is below 2×10^{-3}m, so let $r = 1.5 \times 10^{-4}$m and $r = 2 \times 10^{-3}$m [44]. Substituting these parameter values into Eq. (12), we get the acceleration motion time of bubble with these two radii as shown in Fig. 5.

From Fig. 5, when $r = 1.5 \times 10^{-4}$m and $t_d = 1 \times 10^{-6}$s, $y \to 0$. when $r = 2 \times 10^{-3}$m and $t_d = 1.5 \times 10^{-4}$s, $y \to 0$. This means that it takes quite a short time for bubble to reach v_{max}, then the bubble starts a uniform linear ascending motion. Therefore, t_d can be neglected, and the bubble acceleration movement can be ignored accordingly.

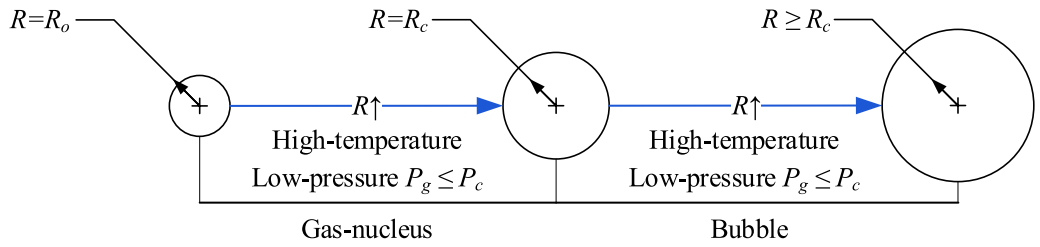

FIGURE 3. Gas-nucleus developing into bubble.

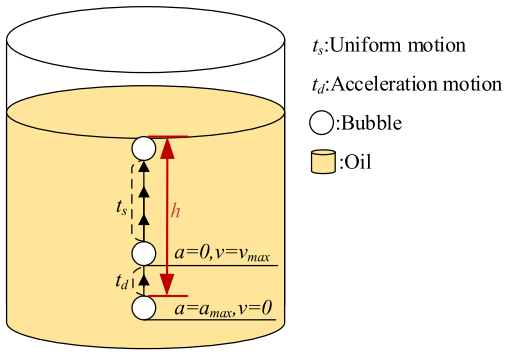

FIGURE 4. Bubble ascending process in hydraulic oil.

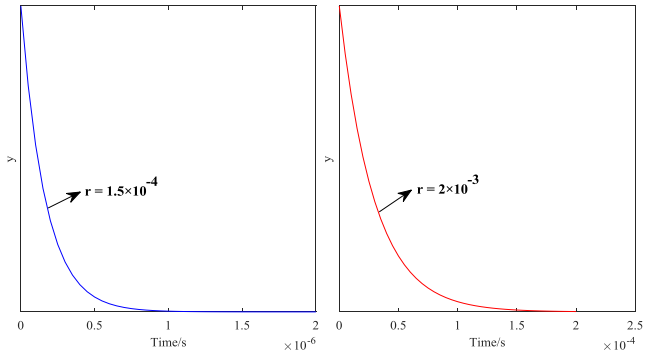

FIGURE 5. Acceleration motion time of bubble.

In short, the rising motion of the bubble can be simplified to a uniform motion of $v = v_{max}$, as shown in Fig. 6. The bubble rising speed mentioned later is v_{max}.

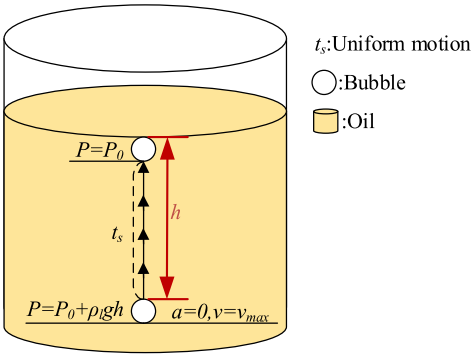

FIGURE 6. Simplified bubble ascending process in hydraulic oil.

According to Eq. (3):

$$P_b = P_0 + \rho_l g h \tag{13}$$

$$n_b = \frac{m}{M_b} \tag{14}$$

$$V_b = \frac{4}{3}\pi r^3 \tag{15}$$

Substituting Eqs. (13)- (15) into Eq. (3) is

$$r = \sqrt{\frac{3mR_mT}{4\pi M_b(P_0 + \rho_l g h)}} \tag{16}$$

where m, R, T, ρ_l, h, M are constants. With the increase of T and decrease of P_0, r will be increased. This further proves that in HTV environment, the radius of bubble will become larger, and its buoyancy will be increased.

It can be seen from Eq. (11) that the bubble rising speed is affected by oil viscosity. Oil viscosity is associated with ambient temperature and pressure. In HTV environment, oil is expanded, molecular spacing is increased, and molecular attraction is decreased, so oil viscosity is decreased as well [45], [46]. This viscosity change law can be expressed as:

$$u = u_0 e^{\alpha P_0 - \lambda(T - T_0)} \tag{17}$$

In Eq. (20), α, λ, T_0, and u_0 are constants. When T is increased and P_0 is decreased, u will be decreased.

Then:

$$\rho_g = \frac{m}{V_b} = \frac{3m}{4\pi r^3} \tag{18}$$

Substituting Eq. (18) into Eq. (11) is

$$v_{\max} = \frac{2g\rho_l}{9u} r^2 - \frac{mg}{6u\pi} r^{-1} \tag{19}$$

Then:

$$t_s = \frac{h}{v_{\max}} \tag{20}$$

Therefore, in HTV environment, r will be increased and u will be decreased, which makes v_{max} to be increased and t_s to be decreased. These result in shortened bubble rising time, indicating that bubble will quickly float to oil surface and be released.

C. DEWATERING

The principle of water removal in hydraulic oil is to utilize the differences of saturated vapor pressure (SVP) of hydraulic oil and water during vacuum heating [47], [48]. In closed environment at certain temperature, the pressure of vapor in equilibrium with liquid is called SVP. Different liquids have

different SVPs and the SVP of the same liquid increases as temperature becomes higher [49], [50]. Both boiling-point and volatility of liquid are related to SVP [51], [52]. For different liquids at the same temperature, the higher the SVP is, the lower the boiling point and the stronger the volatility are. Now take commonly used No. 32, 46, 68, 100, 150 anti-wear hydraulic oil and water as examples for comparison, and list their SVPs at 20°C and 60°C in Table 3 [53], [54]. Apparently, the SVP of water is much higher than that of hydraulic oil. When hydraulic oil is heated under vacuum, the water in it is more prone to be volatile. Therefore, water could be both separated and removed from hydraulic oil by vacuum heating at certain temperature.

TABLE 3. SVP of hydraulic oil and water.

	V-32	V-46	V-68
20°C	1.9×10^{-3}Pa	2.0×10^{-3}Pa	2.3×10^{-3}Pa
60°C	4.0×10^{-3}Pa	2.5×10^{-3}Pa	4.5×10^{-4}Pa
	V-100	V-150	Water
20°C	1.1×10^{-7}Pa	8.0×10^{-9}Pa	2.339×10^{3}Pa
60°C	4.0×10^{-5}Pa	3.3×10^{-6}Pa	1.9932×10^{4}Pa

It is known that high temperature easily causes oil molecules to polymerize into resin substances, such as asphalt or tar, which easily block oil pipes and oil filters, and finally affect the work of the MOIE [55]. The service life of hydraulic oil is closely related to its work temperature. When temperature is higher 60°C, every 8°C increase will shorten its service life by half. The lifespan of oil at 90°C is only 10% of it at 60°C [56]. Choose an appropriate work temperature which allows water to be heated and separated from oil while ensuring sufficient oil serving time is critical.

The SVP of water and commonly used oil at 60°C is 19.932×10^{3}Pa and less than 4.0×10^{-3}Pa, respectively. This vacuum refers to the middle level of vacuum degree, between 1.333×10^{-1}Pa and 1.333×10^{3}Pa. When hydraulic oil is in a vacuum environment of 60°C, water molecules will volatilize to form gas-nucleus, while oil molecules remain stable. Therefore, 60°C is selected as the temperature for degassing and dewatering from hydraulic oil.

III. DESIGN OF THE MOIE

Based on the theoretical analysis described in Section II, the MOIE that integrates oil absorption, removing solid particles, degassing, dewatering and oil-injection functions can be designed.

A. GENERAL DESIGN

The MOIE can be decomposed into four parts, including the oil filter system, the pressure tank system, the vacuum pump system, and the equipment trolley. The oil filter system is mainly used to filter solid particles in hydraulic oil. The pressure tank system is a vacuum heating chamber for degassing and dewatering of hydraulic oil. The vacuum pump system extracts gas from the pressure tank to ensure the low pressure inside of the pressure tank. The equipment trolley fixes devices and makes it portable. The function of each MOIE system is shown in Fig. 7.

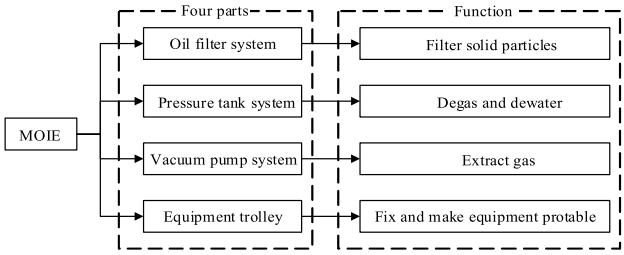

FIGURE 7. Function of each system in the MOIE.

The MOIE consists of a vacuum pump, high-precision oil filter, two immersion electrical heaters, some measuring gauges, a pressure tank with capacity of 60L and inner diameter of 0.5m, etc. Fresh air can be injected into the pressure tank through an air filter. The heater located near the bottom of tank has the maximum power of 2kw and can be adjusted by a designed program. To let oil be heated evenly, the inner circulation is ensured during the heating process. The hydraulic oil circuit of the MOIE is shown in Fig. 8, and the crucial steps of the oil purification process are explained here.

1) Oil absorption and filtration. Connect the oil inlet pipe to an external oil tank. Open the vacuum pump to vacuumize the pressure tank. The air pressure in the external tank is higher than that in the pressure tank. Due to such pressure difference, the oil will flow into the pressure tank along the oil pipe. Switch on the low-pressure oil transfer pump to enhance the oil transfer capacity and the internal circulation capacity. After the oil passes through the paper oil filter, the solid particles in the oil will be filtered.

2) Degassing and dewatering. Switch off the oil inlet valve once the volume of oil in the pressure tank reaches the preset value. Keep the vacuum pump running to maintain a low pressure in the pressure tank. Switch on the electric heaters and heat the oil according to the preset control program to keep the oil temperature at 60°C. It starts degassing and dewatering.

3) Oil injection. Use vacuum oil injection to complete oil filling operation. First, vacuum the hydraulic equipment to evacuate the residual air in the hydraulic equipment and keep it as well as the pressure tank in vacuum state. Second, switch on the oil valve between the pressure tank and the hydraulic equipment. There is a height difference between them. Based on the law of connected vessels, when the air pressure in the hydraulic equipment and the pressure tank are the same, their liquid within reaches the same level. Therefore, the oil in the pressure tank will flow into the hydraulic equipment via the oil pipe.

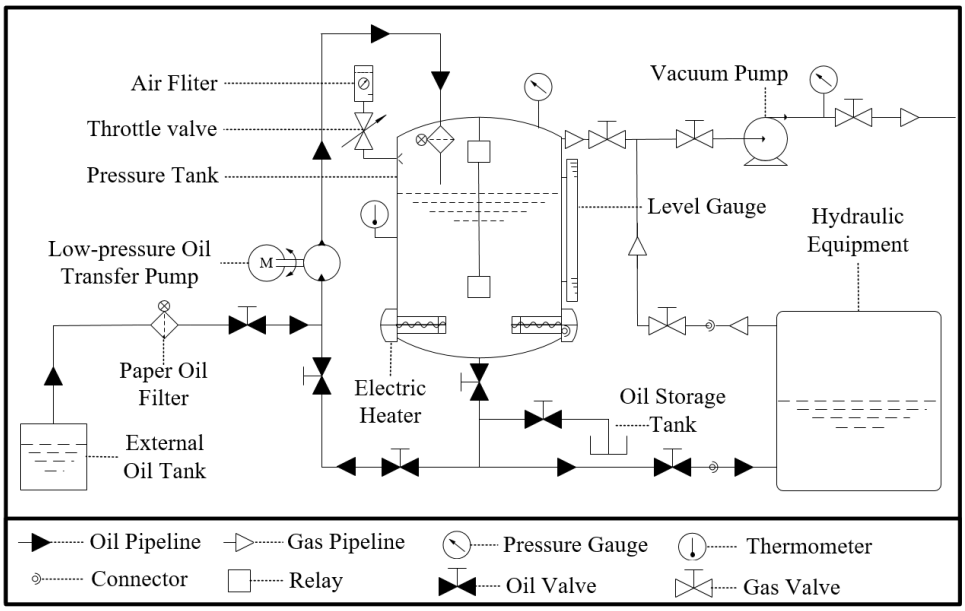

FIGURE 8. Hydraulic oil circuit of the MOIE.

B. DESIGN OF THE PRESSURE TANK IN THE MOIE

This section focuses on the design of the pressure tank, one of the crucial steps in designing the MOIE. The following mainly introduces the pressure tank material, thickness, temperature control system, heater, air filter.

Stainless steel 304 is renowned for rust prevention, oxidation resistance, high-temperature resistance and corrosion resistance [57], [58]. It is selected as the material of the pressure tank wall. Wall thickness is the most important structural parameter of pressure tank. Appropriate wall thickness is the basic condition for ensuring structural strength, structural rigidity and service life [59], [60]. The calculation of the pressure tank wall thickness is closely related to the allowable stress:

$$\begin{cases} [\sigma_{amin}] = \dfrac{\sigma_{amin}}{n_s} = \dfrac{310}{3} = 103.3\text{MPa} \\ [\sigma_{bmin}] = \dfrac{\sigma_{bmin}}{n_s} = \dfrac{620}{3} = 206.7\text{MPa} \end{cases} \tag{21}$$

The description of all the parameters from Eq.s (21) to (25) and their numerical values are provided in Table 4. In Eq. (21), $[\sigma amin]$ is the allowable stress of the yield limit, and $[\sigma bmin]$ is the allowable stress of the tensile limit, so the allowable stress $[\sigma] = 103.3\text{MPa}$.

Calculate the wall thickness of the pressure tank as shown in Eq. (25):

$$\begin{cases} \delta_n = \delta + C + \Delta \\ \delta \geq \dfrac{P_{i\max} \cdot d}{2[\delta] - p_{imax}} = \dfrac{0.5 \times 490}{2 \times 103.3 \times 1 - 0.5} \\ \quad = 1.189mm \\ C = C_1 + C_2 \end{cases} \tag{22}$$

where δ_n is the wall thickness of the pressure tank, δ is the calculated thickness, and C is the additional thickness. The calculated thickness is to ensure the strength and stiffness of the container under specified load conditions. According to GB150 $\sim$ 89, it refers to the ASME code and the Japanese JISB8243 code equivalent to ASME [61], [62]. The additional thickness C is divided into C_1 and C_2. C_1 is the negative thickness deviation of steel plate and C_2 is the corrosion allowance [63], [64]. During rolling procedure of manufacturing processes, the thickness of pressure tank may vary. If negative deviation occurs, the actual thickness will be smaller than it is calculated, and the strength of pressure tank might be affected accordingly. Therefore, a negative thickness deviation C_1 is introduced to increase the thickness in advance. The relationship between the values in the pressure tank thickness calculation is shown in Fig. 9.

Because of the corrosion resistance of 304 stainless steel, we assume hydraulic oil to be non-corrosive, $C_2 = 0$. Now take $C = 1.25\text{mm}$, round δ_n to 2.5mm. Then calculate the maximum withstood pressure:

$$\begin{cases} \delta_e = \delta_{\text{n}} - C = 2.5\text{-}1.25 = 1.25\text{mm} \\ P_{\text{amax}} = \dfrac{2\delta_e [\sigma] \varphi}{d + \delta_e} = \dfrac{2 \times 1.25 \times 103.3 \times 1}{490 + 1.25} \\ \quad = 0.526\text{MPa} \end{cases} \tag{23}$$

where δ_e is the effective thickness, and P_{amax} is the actual maximum withstood pressure. Here, P_{amax} is almost close to P_{imax}, so the wall thickness of the pressure tank $\delta_n = 5\text{mm}$ is considered reasonable and feasible.

As explained in Section II, excessively high oil-temperature would damage the quality of hydraulic oil, and excessively low oil-temperature would cause difficulty to achieve degassing and dewatering. Therefore, the temperature of hydraulic oil must be strictly controlled. The heater installed inside the pressure tank is used to heat the hydraulic

TABLE 4. Description of parameters.

Notation	Description	Value	Notation	Description	Value
σ_{amin}	Yield limit of stainless steel 304	310MPa	C_o	Specific heat capacity of oil	1.8×10^3J/(kg·°C)
σ_{bmin}	Tensile limit of stainless steel 304	620MPa	γ	Oil density	900kg/m^3
n_s	Safety factor	3	V	Oil volume in the fuel tank	0.06m^3
φ	Weld coefficient	1	ΔQ	Temperature difference	40°C
d	Inner diameter of the tank	490mm	T	Heating time	3600s
C	Thickness additional	1.5mm	η	Heating efficiency	0.7
δ_n	Nominal thickness	5mm	P_{imax}	Ideal maximum withstand pressure	0.5MPa

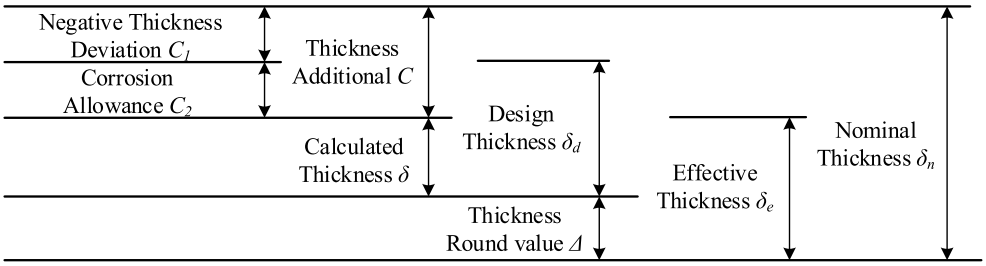

FIGURE 9. Pressure tank thickness.

oil up to a temperature of 60°C. This paper adopts the modified Smith fuzzy PID controller to maintain the oil temperature at 60°C, and the oil heating system is the control object. The transfer function as a first-order transfer function with a delay described by Huang et.al. is shown in Eq. (24), which not only reserves the main features of controlled object but also facilitates the theoretical analysis and the real control operation [65], [66].

$$G(s) = \frac{22.8}{451.85s + 1} e^{-77.11s} \tag{24}$$

With the characteristics of large inertia, large time delay and large time-varying parameters, it is difficult for traditional PID controller to control accurately the oil heating process in the MOIE [67]. The traditional Smith predictor can solve such problems, but must obtain accurate mathematical models of the controlled system. To further reduce the accuracy requirements of the model and obtain better control results, a first-order filter is added to the Smith predictor [65]. And the block diagram of the modified Smith fuzzy PID control system is shown in Fig. 10.

The modified Smith fuzzy PID control system not only maintains the dynamic performance advantages of the Smith fuzzy PID control, but also has good robustness and small oscillation. Therefore, it can meet the requirements of the temperature control for degassing and dewatering of hydraulic oil. The heating power of the heater can be

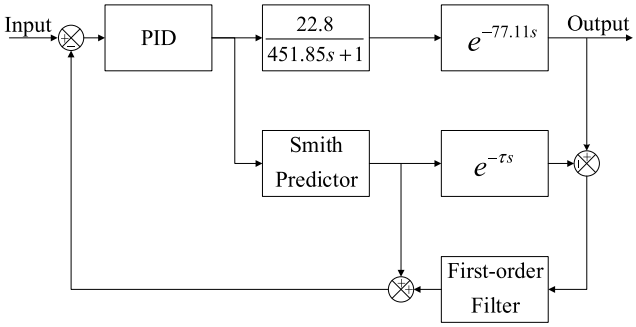

FIGURE 10. Block diagram of the modified Smith fuzzy PID control system.

estimated by Eq. (28):

$$\begin{cases} N \geq \dfrac{C_o \cdot \gamma \cdot V \cdot \Delta Q}{T} = 1.08\text{KW} \\ P = \dfrac{N}{\eta} = 1.54\text{KW} \end{cases} \tag{25}$$

where N is the energy required for the pressure tank, and P is the power required by the heater. The normal temperature of hydraulic oil is about 20°C, so the temperature difference ΔQ is 40°C. Hence, it is necessary to select the heater with the power greater than 1.54KW to meet the requirement. Two heaters with the specification of GYY2-220/1 are selected with the power of each 1KW.

The pressure tank is also equipped with level gauge, thermometer, air filter, relay, pressure gauge, etc. The 3D model of the pressure tank is displayed in Fig. 11. When sucking

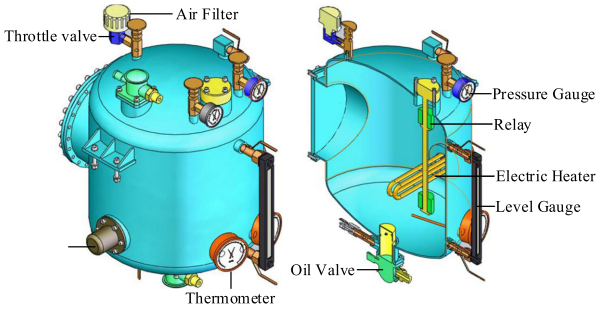

FIGURE 11. 3D model of the pressure tank.

FIGURE 12. Prototype of the MOIE.

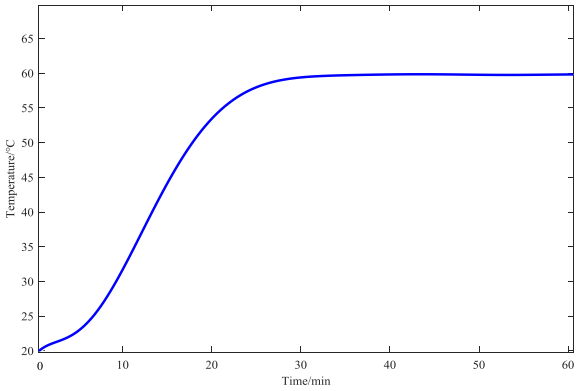

FIGURE 13. Oil temperature change with time.

oil, the low-pressure oil pump will ensure that the hydraulic oil circulates in the low-pressure oil circuit. However, if the gas pressure in the pressure tank is too low, the self-priming ability of the low-pressure oil pump will be reduced, and even bubble will be generated. The gas remaining in the MOIE before its working may be dissolved in hydraulic oil, so all the gas needs to be discharged through the vacuum pump. After the gas is discharged, the inside of the MOIE is in vacuum, which is not conducive to the work of the low-pressure oil pump. Therefore, to ensure the gas pressure not too low, an air filter is installed on the top of pressure tank to communicate with the atmosphere. The gas from the air filter will not be dissolved into the hydraulic oil, and only a small amount of gas can enter the pressure tank through the throttle valve control. After the oil suction is completed, the throttle valve will be closed to prevent gas entering the pressure tank. Therefore, the vacuum degree of the pressure tank is safely ensured.

IV. EXPERIMENTS

This section verifies the oil purification performance of the MOIE by a series of degassing and dewatering experiments carried out in the laboratory at the Ocean College of Zhejiang University. The prototype of the MOIE is displayed in Fig. 12. The oil temperature change curve of the pressure tank when the MOIE works is shown in Fig. 13. After the MOIE runs for 30 minutes, the temperature can reach to and maintain at 60°C. Therefore, the degassing and dewatering experiment time was set for 60 minutes to allow gas and water to be maximally removed. The hydraulic oil used in the experiment was No. 46 anti-wear hydraulic oil. Each sample in both degassing and dewatering experiment was repeated for 20 times. Record the results of each time, and take the median of density in degassing experiment and the median of volume in dewatering experiment as the representative of each sample for later analysis.

A. DEGASSING EXPERIMENT

The degassing performance of the MOIE is verified by measuring and comparing the density of the hydraulic oil. First, four samples with 500ml hydraulic oil for each were prepared. Secondly, these samples were undergoing different processes as described in Table 5. Finally, the degassing effect of the MOIE was evaluated by calculating and comparing the density of each sample.

TABLE 5. Degassing experiment.

Sample	Operation	Time
1	Oil only passes through the high-precision oil filter	Stand for 60 minutes
2	Turn on the low-pressure oil transfer pump and oil passes through the high-precision oil filter	Stand for 60 minutes
3	MOIE starts working but switch off electric heater (Vacuum but no heating)	Work for 60 minutes.
4	MOIE works normally (Vacuum heating at 60 °C)	Work for 60 minutes.

To prevent air contacting hydraulic oil when measuring the volume of hydraulic oil, we designed a graduated cylinder as shown in Fig. 14. The top of the graduated cylinder is semi-closed only allowing oil pipeline of the MOIE to enter. Before starting the measurement, the air in the graduated cylinder is evacuated through an injection syringe.

The experimental results are presented as follows:

1) At the beginning, sample 1contained a small amount of large bubbles. After being placed for 60 minutes, the bubbles were partially released. Its mass was measured as 441.89g and its density was calculated to be 0.88378g/cm^3.

2) Sample 2 contained fine bubbles and it is difficult to release them by purely standing still, as shown in Fig. 15. Its

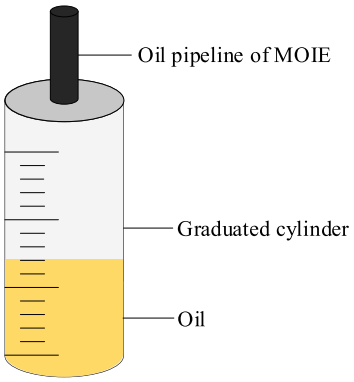

FIGURE 14. Graduated cylinder.

mass was measured as 439.93g, and its density was calculated to be 0.87986g/cm^3.

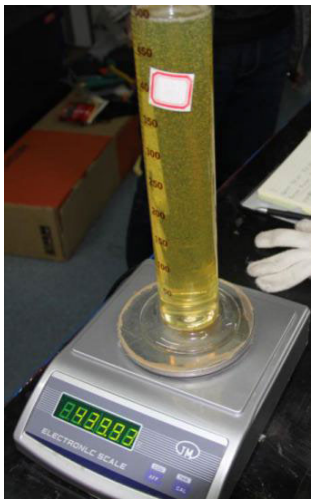

FIGURE 15. Sample 2 in degassing experiment.

3) There were no visible bubbles in Sample 3. Its mass was measured as 441.99g, and its density was calculated to be 0.88398g/cm^3.

4) There were no visible bubbles in sample 4 neither. Its mass was measured as 442.44g, and its density was calculated to be 0.88488g/cm^3.

The calculated density of each sample is plotted and displayed in Fig. 16. The following conclusions can be drawn.

1) The density of sample 2 is significantly low. This indicates that when the hydraulic oil flows through the low-pressure oil transfer pump, a small amount of air is mixed inside. Therefore, after the MOIE sucks oil, the gas content of the hydraulic oil in the pressure tank becomes higher.

2) The density of sample 3 is similar to sample 1. This indicates that only 60 minutes' vacuum treatment of the hydraulic oil does not achieve effective degassing.

3) Compared with the other three samples, sample 4 has the highest density, which indicates that the purity of hydraulic oil in sample 4 is the best. This verifies that the hydraulic oil is degassed in a vacuum environment of 60°C. And it also proves that the degassing function of the MOIE is feasible and effective.

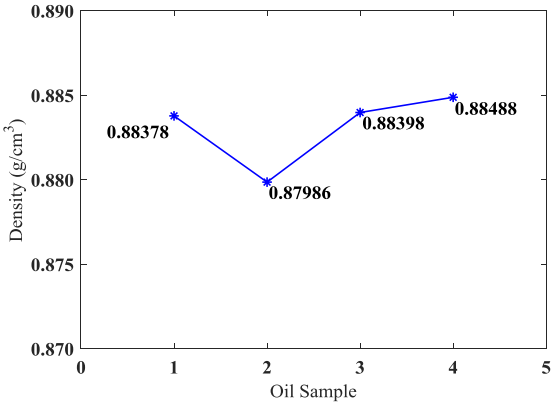

FIGURE 16. Each sample density.

B. DEWATERING EXPERIMENT

The dewatering performance of the MOIE is verified by measuring and comparing the turbidity of the hydraulic oil. Firstly, three samples were prepared with 240ml hydraulic oil in the first sample and 210ml in the rest two. Different operations were performed on each sample as described in Table 6. Then, the dewatering effect of the MOIE was verified by comparing the turbidity of each sample. To clearly compare and analyze the experiment results, sample 2 and 3 were added 30ml water, respectively. Then the hydraulic oil was emulsified and appeared milky and turbid, as shown in sample 2 in Fig. 17.

TABLE 6. Degassing experiment.

Sample	Type of hydraulic oil	Operating
1	240ml of the original hydraulic oil	Static
2	Mix 210ml of the original hydraulic oil and 30ml of water together and stir.	Static
3	Mix 210ml of the original hydraulic oil and 30ml of water together and stir	MOIE works normally

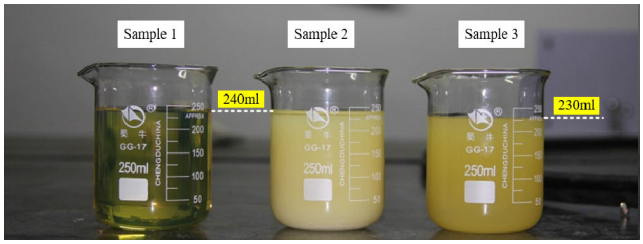

FIGURE 17. Dewatering experiment.

Compared with sample 1, sample 2 is apparently found to be of a higher turbidity. Compared with sample 2, the turbidity of sample 3 was lower, and its liquid was 10 ml less than that of sample 2. It indicates that after the MOIE worked for 60 minutes, 10ml of water in the hydraulic

oil was removed, and the dewatering rate reached 33.33%. Since most hydraulic oil contains less than 0.01% of water, the dewatering performance of the MOIE is regarded feasible and sufficient.

V. CONCLUSION

In this paper, the MOIE, multifunctional oil-injection equipment for deep-sea hydraulic systems, is proposed. Its major functions are to absorb oil, remove impurities and fill oil, among which the removal of impurities is of significance and is achieved through vacuum filtration and vacuum heating. The prototype was designed and developed, and the laboratory-based experiments were carried out to further verify the degassing and dewatering performance of the MOIE. Based on this, the following conclusions are drawn:

1) Both theory and experiment have proved that the paper oil filter is suitable in the MOIE.

2) In high-temperature and low-pressure environment, hydraulic oil can be degassed and dewatered, and at a temperature of 60°C, the MOIE works best.

3) The design of the pressure tank is crucial, and its wall thickness has been calculated to be 5mm. The modified Smith fuzzy PID controller can achieve temperature control, maintaining the internal temperature of the pressure tank at 60°C.

4) The laboratory experiments have proved that hydraulic oil can be degassed and dewatered by the MOIE with vacuum heating.

Through the experiments we find that the control system of the MOIE still needs improvement. When it works for more than 18 hours, the preset temperature cannot be stably kept. At this time, it needs to be revised manually. For future work, more experiments are expected to improve the reliability of the MOIE.

REFERENCES

[1] X.-P. Cao, M. Ye, B. Deng, C.-H. Zhang, and Z.-Y. Yu, "LVP modeling and dynamic characteristics prediction of a hydraulic power unit in deep-sea," *China Ocean Eng.*, vol. 27, no. 1, pp. 17–32, Mar. 2013.

[2] H. Wu, B. Jin, C. Yang, and Y. Chen, "Modeling and application of pressure compensation device of the deep-sea hydraulic system," *Hydraul. Pneum.*, vol. 9, no. 2, pp. 46–49, 2010.

[3] L. Zeng, H. Zhang, X. Zhao, and H. Teng, "Double coil multi-parameter impedance sensor for hydraulic oil pollutants detection," *Chin. J. Sci. Instrum.*, vol. 38, no. 7, pp. 1690–1697, Apr. 2017.

[4] R.-C. Zhang, X. Yu, Y.-L. Hu, H.-J. Zang, and W. Shu, "Active control of hydraulic oil contamination to extend the service life of aviation hydraulic system," *Int. J. Adv. Manuf. Technol.*, vol. 96, nos. 5–8, pp. 1693–1704, May 2018.

[5] M. Cai, S. Wu, and C. Yang, "Effect of low temperature and high pressure on deep-sea oil-filled brushless DC motors," *Mar. Technol. Soc. J.*, vol. 50, no. 2, pp. 83–93, Mar. 2016.

[6] F. Ng, J. A. Harding, and J. Glass, "Improving hydraulic excavator performance through in line hydraulic oil contamination monitoring," *Mech. Syst. Signal Process.*, vol. 83, pp. 176–193, Jan. 2017.

[7] Z. H. Zhang, S. L. Nie, L. M. Zhang, and S. H. Yuan, "Development of seawater hydraulic pump tester in deep-sea simulated environment," in *Proc. Int. Conf. Fluid Power Mechatronics (FPM)*, Aug. 2015, pp. 667–671.

[8] R. Mettin and C. Cairós, "Bubble dynamics and observations BT," in *Handbook of Ultrasonics and Sonochemistry*. Singapore: Springer, 2016, pp. 3–31.

[9] Z. Qifeng, Z. Yunxiu, H. Liangqing, K. Fandong, D. Linsen, C. Shengguo, and Z. Yang, "Design and pressure experiments of a deep-sea hydraulic manipulator system," in *Proc. Int. Conf. Intell. Robot. Appl.*, 2014, pp. 117–128.

[10] E. S. Barkan and D. A. Sheinin, "A general technique for the calculation of formation conditions of natural gas hydrates," *Fluid Phase Equilibria*, vol. 86, pp. 111–136, Jul. 1993.

[11] N. S. Dhillon, J. C. Cheng, and A. P. Pisano, "Device packaging techniques for implementing a novel thermal flux method for fluid degassing and charging of a planar microscale loop heat pipe," in *Proc. ASME Int. Mech. Eng. Congr. Expo.*, vol. 11, 2011, pp. 963–971.

[12] Y. Gerner, C. W. Sims, and J. Thompson, "Method for degassing a fluid," Google Patents US 7 947 112 B1, May 24, 2011.

[13] Q. Yang, X. Xu, H. Lu, and C. Wang, "Apparatus for liquid degassing using coupling of swirling flow or centrifugal field and pressure gradient field," U.S. Patent Appl. 14 764 179, Mar. 24, 2016.

[14] M. Nüllig and F. Peters, "Experiments on the mass transfer of gas bubbles in mineral oil," *Colloids Surf. A, Physicochem. Eng. Aspects*, vol. 540, pp. 81–89, Mar. 2018.

[15] X. Xu, H. Lu, Y. Qian, B. Zhang, H. Wang, H. Liu, and Q. Yang, "Gas-liquid mass transfer and bubble size distribution in a multi-cyclone separator," *AIChE J.*, vol. 65, no. 1, pp. 221–229, Jan. 2019.

[16] N. K. Myshkin and L. V. Markova, "Monitoring of water content in oil," in *On-line Condition Monitoring in Industrial Lubrication and Tribology*. Cham, Switzerland: Springer, 2018, pp. 61–81.

[17] R. W. Lin, "Removal of water from bio-oil," U.S. Patent 8 083 900, Dec. 27, 2011.

[18] J. Pfaffenberger and D. S. Mackenzie, "Methods of water removal from quench oils," in *Proc. Thermal Process. Motion-Including Int. Conf. Heat Treatment Surf. Eng. Automot. Appl.*, 2018, pp. 106–111.

[19] Q. Wang, J. Duanmu, Z. Zhu, and X. Ge, "Oil filter debris analysis of aero-engine," in *Proc. 9th Int. Conf. Rel., Maintainability Saf.*, Jun. 2011, pp. 276–278.

[20] M. Reik and F. Oberli, "Selection of filters for lubricating oil and hydraulic systems BT," in *Encyclopedia of Lubricants and Lubrication*, T. Mang, Ed. Berlin, Germany: Springer, 2014, pp. 1710–1720.

[21] D. B. Harder, P. E. Johnson, E. Stenersen, C. A. Rausch, and J. R. Hacker, "Fluid filter and methods," U.S. Patent 7 556 155, Jul. 7, 2009.

[22] V. S. Shagapov, V. V. Koledin, and N. K. Vakhitova, "Stability of an overheated liquid containing vapor-gas bubbles," *J. Appl. Mech. Tech. Phys.*, vol. 54, no. 5, pp. 742–755, Sep. 2013.

[23] S. Pan and O. Jun, "Observation and analysis of going-up movement of bubbles," *J. Wuhan Univ. Hydraul. Electr. Eng.*, vol. 4, no. 2, pp. 40–47, 1993

[24] H. Jing-chuan, "Conditions for incipient cavitation formation," *Appl. Math. Mech.*, vol. 10, no. 2, pp. 163–166, Feb. 1989.

[25] E. B. Flint and K. S. Suslick, "The temperature of cavitation," *Science*, vol. 253, no. 5026, pp. 1397–1399, 1991.

[26] S. Pan, "Spectrum of distribution of gas nucleus scale," *J. Hydrodyn.*, vol. 2, no. 2, p. 57, 1987.

[27] G. L. Chahine, "Numerical simulation of bubble flow interactions," *J. Hydrodyn.*, vol. 21, no. 3, pp. 316–332, Jun. 2009.

[28] Q. Yang, J. Zhang, G. Dai, H. Wang, and J. Wu, "Influence of gas nucleus on scale effect of cavitation," *Shuili Fadian Xuebao/J. Hydroelectr. Eng.*, vol. 24, no. 3, pp. 75–92, 2005.

[29] B. Gindroz, J.-Y. Billard, and P. Geistdoerfer, "Cavitation nuclei measurements at sea," Amer. Soc. Mech. Eng., Heat Transf. Division, American, Tech. Rep., 1995, pp. 464–471, vol. 321, no. 2.

[30] Y.-L. Zhang, W.-L. Xu, F.-X. Zhang, and Q. Zhang, "Collapsing characteristics of gas-bearing cavitation bubble," *J. Hydrodyn.*, vol. 31, no. 1, pp. 66–75, Feb. 2019.

[31] V. S. Shagapov, M. N. Galimzyanov, and I. I. Vdovenko, "Characteristics of the stability and acoustic properties of superheated liquid with gas nuclei under increasing pressure," *High Temp.*, vol. 57, no. 5, pp. 712–717, Sep. 2019.

[32] J. P. Franc and J. M. Michel, "Fundamentals of cavitation," *Fluid Mech. Appl.*, vol. 76, no. 11, pp. 205–217, 2005.

[33] M. S. Plesset and A. Prosperetti, "Bubble dynamics and cavitation," *Annu. Rev. Fluid Mech.*, vol. 9, no. 1, pp. 145–185, 2003.

[34] H. Jing-Chuan and H. Cheng-Cai, "Influences of gas nucleus scale on cavitation," *Appl. Math. Mech.*, vol. 13, no. 4, pp. 359–367, Apr. 1992.

[35] F. Qiang, C. Ming, W. Xiuli, Z. Rongsheng, Z. Guoyu, and Y. Jianen, "Stability of air nucleus in liquid water and cavitation inception on marine engineering," *Polish Maritime Res.*, vol. 25, no. 3, pp. 111–119, Dec. 2018.

[36] G. L. Chahine, "Bubble interactions with vortices BT," in *Fluid Vortices*, S. I. Green, Ed. Dordrecht, The Netherlands: Springer, 1995, pp. 783–828.
[37] S. Sasaki, K. Hayashi, and A. Tomiyama, "Effects of liquid height on gas holdup in air–water bubble column," *Exp. Thermal Fluid Sci.*, vol. 72, pp. 67–74, Apr. 2016.
[38] R. van Hout, A. Gulitski, D. Barnea, and L. Shemer, "Experimental investigation of the velocity field induced by a Taylor bubble rising in stagnant water," *Int. J. Multiphase Flow*, vol. 28, no. 4, pp. 579–596, Apr. 2002.
[39] C. Pesci, A. Weiner, H. Marschall, and D. Bothe, "Computational analysis of single rising bubbles influenced by soluble surfactant," *J. Fluid Mech.*, vol. 856, pp. 709–763, Dec. 2018.
[40] R. Lindken and W. Merzkirch, "Velocity measurements of liquid and gaseous phase for a system of bubbles rising in water," *Exp. Fluids*, vol. 29, no. 7, pp. S194–S201, Dec. 2000.
[41] D. R. Adkins, K. A. Shollenberger, and J. R. Torczynski, "Pressure effects on bubble-column flow characteristics," in *Proc. Ans*, 1996, pp. 1–15.
[42] W. Cheng, X. Zhou, J. Guo, and L. I. Hua, "Experimental study of the velocity of bubble rising in water," *J. Xian Univ. Technol.*, vol. 16, no. 1, pp. 57–60, 2000.
[43] T. Uemura, M. Iguchi, and Y. Ueda, "Behavior of a rising bubble through an oil/water interface BT," in *Flow Visualization in Materials Processing: Practical Techniques and Selected Applications*, T. Uemura, Y. Ueda, and M. Iguchi, Eds. Tokyo, Japan: Springer Japan, 2018, pp. 89–115.
[44] M. Wu and M. Gharib, "Experimental studies on the shape and path of small air bubbles rising in clean water," *Phys. Fluids*, vol. 14, no. 7, pp. L49–L52, 2002.
[45] K. L. Husan, *Fluid Mechanics: Theory and Problems*. New Rochelle, NY, USA: Intelliz Press, 2018.
[46] Y. Zhang, A. Sam, and J. A. Finch, "Temperature effect on single bubble velocity profile in water and surfactant solution," *Colloids Surf. A, Physicochem. Eng. Aspects*, vol. 223, no. 1, pp. 45–54, 2003.
[47] O. S. Vitkovskii, "Measuring the saturated vapor pressure of oil and petroleum products: Current status and future development," *Meas. Techn.*, vol. 57, no. 5, pp. 577–579, Aug. 2014.
[48] A. Roosta and J. Hekayati, "A simple generic model for estimating saturated vapor pressure," *Chem. Eng. Commun.*, vol. 203, no. 8, pp. 1020–1028, Aug. 2016.
[49] I. N. Buneev, A. A. Gureev, M. I. Fal'kovich, and V. T. Solodovnikova, "Effect of temperature on the viscosity and saturated vapor pressure of vacuum oils," *Chem. Technol. Fuels Oils*, vol. 27, no. 9, pp. 492–495, Sep. 1991.
[50] A. Y. Nikiforov, "Plasma sputtering of water molecules from the liquid phase by low-energy ions: Molecular dynamics simulation," *High Energy Chem.*, vol. 42, no. 3, pp. 235–239, May 2008.
[51] E. Wilhelm and T. M. Letcher, *Volume Properties: Liquids, Solutions and Vapours*. Cambridge, U.K.: The Royal Society of Chemistry, 2015.
[52] V. Thomsen, "The boiling point of water," *Phys. Teach.*, vol. 35, no. 2, pp. 98–99, 1997.
[53] W. Bock, "Hydraulic fluids," in *Encyclopedia of Lubricants and Lubrication*. Berlin, Germany: Springer, 2014.
[54] V. N. Gorobei, M. P. Krutovskikh, and O. S. Vitkovskii, "Measurement methods and instruments for the saturated vapor pressure of oil products," *Meas. Techn.*, vol. 49, no. 3, pp. 265–269, Mar. 2006.
[55] Y. M. Ganeeva, T. N. Yusupova, V. I. Morozov, and G. V. Romanov, "Self-organization behavior of asphaltene molecules in heavy oils with varying the oil: Precipitant ratio," *Petroleum Chem.*, vol. 53, no. 4, pp. 220–224, Jul. 2013.
[56] V. A. Tyshchenko, T. N. Shabalina, E. V. Lobzin, A. A. Polyakova, and L. D. Kalinina, "Evaluation of hydraulic oil aging," *Chem. Technol. Fuels Oils*, vol. 29, no. 7, pp. 355–358, 1993.
[57] Y. Isshiki, J. Shi, H. Nakai, and M. Hashimoto, "Microstructure, microhardness, composition, and corrosive properties of stainless steel 304 II. Low-pressure laser spraying with silicon," *Appl. Phys. A, Mater. Sci. Process.*, vol. 70, no. 6, pp. 651–656, Jun. 2000.
[58] J. Lee, Y. Choi, C. Jo, and D. Chang, "Design of a prismatic pressure vessel: An engineering solution for non-stiffened-type vessels," *Ocean Eng.*, vol. 142, pp. 639–649, Sep. 2017.
[59] S. Zhang, H. Li, X. Zhao, Z. Yuan, S. Hao, H. Huang, J. Leng, Y. Jiang, Y. Shen, and C. Zhang, "A multifunctional oiling equipment for deep-sea hydraulic system," in *Proc. OCEANS*, Anchorage, AK, USA, Sep. 2017, pp. 1–5.
[60] L. I. Huan, Y. Wei, J. Shi, and F. Liang, "The finite element analysis of pressure vessel wall thickness," *J. Yunnan Agric. Univ.*, vol. 123, no. 4, pp. 85–88, 2014.
[61] L. Gui, T. Xu, Y. Sun, and X. Shang, "Toughness requirement of chinese pressure vessel steel 07mnnimodr based on fracture mechanics assessment method," in *Proc. ASME Pressure Vessels Piping Conf.*, 2018, pp. 1–4.
[62] Y. Sun and P. Wang, "Main influencing factors of hydraulic oil performance for construction machinery," in *Proc. IOP Conf. Ser., Mater. Sci. Eng.*, 2019, vol. 677, no. 2, p. 22129.
[63] D. R. Moss and M. Basic, *Pressure Vessel Design Manual*, 4th ed. Houston, TX, USA: Gulf Publishing, 2013, pp. 743–802.
[64] Y. Liu, "Discussion on additional value C of wall thickness in pressure vessel design," *Press. Vessel*, vol. 21, no. 5, pp. 60–64, 1994.
[65] H. Huang, S. Zhang, Z. Yang, Y. Tian, X. Zhao, Z. Yuan, S. Hao, J. Leng, and Y. Wei, "Modified smith fuzzy PID temperature control in an oil-replenishing device for deep-sea hydraulic system," *Ocean Eng.*, vol. 149, no. 1, pp. 14–22, Feb. 2018.
[66] X. Y. Lou, "Research on oil temperature control technology of mobile machinery in closed hydraulic transmission system," *Adv. Mater. Res.*, vol. 1037, pp. 274–277, Oct. 2014.
[67] X. Dong, "Hydraulic system temperature control," *Bengang Technol.*, vol. 21, no. 5, pp. 36–42, 1995.

HAOCAI HUANG was born in Fujian, China, in 1979. He received the B.S. and M.E. degrees in mechanical engineering from Huaqiao University, China, in 2001 and 2004, respectively, and the Ph.D. degree in mechatronic engineering from Zhejiang University, Zhoushan, China, in 2010. He is currently a Professor with the Ocean College, Zhejiang University. His research interests include ocean technology, ocean observation technology, and ocean bio-robotics.

CHENGCHENG ZHU was born in Fujian, China, in 1996. He received the B.S. degree in automation engineering from Nanjing Agricultural University, Nanjing, China, in 2018. He is currently pursuing the master's degree in naval architecture and ocean engineering with the Ocean College, Zhejiang University, Zhoushan, China. His main research interest includes application in ocean engineering.

WENJUN ZHANG received the B.S. degree in surveying and mapping from Henan Polytechnic University, Jiaozuo, China, in 2012, and the M.Sc. degree in cartography and geographic information engineering from Shandong Technology University, Qingdao, China, in 2015. She is currently pursuing the Ph.D. degree in marine engineering with Harbin Engineering University, Harbin, China. Her current research interest includes ocean technology.

SHUAI HAO received the B.S. degree in electronic science and technology from the University of Electronic Science and Technology of China, Chengdu, China, in 2010, and the M.Sc. degree in marine technology from Zhejiang University, Hangzhou, China, in 2013. Since 2013, she has been with the Ocean College, Zhejiang University, Zhoushan, China, where she is currently an Engineer. Her general research interests include teaching, design, and research in the field.

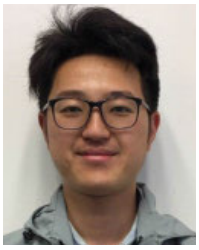

SHUQING ZHANG received the B.S. degree in naval architecture and ocean engineering from the Huazhong University of Science and Technology, in 2015, and the M.Sc. degree in naval architecture and ocean engineering from Zhejiang University, in 2018. His research interests include ocean buoy and mechanical device.

JIANXING LENG received the B.S. degree in naval architecture and ocean engineering from the Jiangsu University of Science and Technology, in 1987, and the M.Sc. degree in naval architecture and ocean engineering and the Ph.D. degree in ship structure analysis from the China Ship Scientific Research Center, in 1992 and 2002, respectively. He was a Senior Researcher and the Director of the Strength Fatigue Testing Station, China Ship Scientific Research Center. Since 2009, he has been with the Ocean College, Zhejiang University, as a Professor, where he is currently the Director of the Engineering Laboratory of Marine Equipment Testing Zhejiang Province. His current research interests include naval architecture, advanced outfitting technology, and underwater sampling devices.

YAN WEI (Member, IEEE) received the B.S. and M.Sc. degrees in naval architecture and ocean engineering from the Wuhan University of Technology, Wuhan, China, in 2004 and 2007, respectively, and the Ph.D. degree in marine technology from the Delft University of Technology, Delft, The Netherlands, in 2012. Since 2012, she has been with the Ocean College, Zhejiang University, Zhoushan, China, where she is currently an Associate Professor. Her general research interests include computational fluid mechanics and its application in ocean engineering, flow-induced noise in underwater acoustic communications, and networking.